Measuring the Mueller matrix of an arbitrary optical element with a universal SU(2) polarization gadget

Salla Gangi Reddy,[1,*] Shashi Prabhakar,[1] A. Aadhi,[1] Ashok Kumar,[2] Megh Shah,[3] R. P. Singh,[1,5] and R. Simon[4,6]

[1]*Physical Research Laboratory, Navarangpura, Ahmedabad 380009, India*
[2]*Instituto de Fisica, Universidade de Sao Paulo, Sao Paulo 66318, Brazil*
[3]*Indian Institute of Technology, Roorkee 247667, India*
[4]*The Institute of Mathematical Sciences, Chennai 600113, India*
[5]*e-mail: rpsingh@prl.res.in*
[6]*e-mail: simon@imsc.res.in*
**Corresponding author: sgreddy@prl.res.in*

Received October 30, 2013; revised January 11, 2014; accepted January 15, 2014;
posted January 17, 2014 (Doc. ID 200448); published February 20, 2014

We propose a new method for determining the Mueller matrix of an arbitrary optical element and verify it with three known optical elements. This method makes use of two universal SU(2) polarization gadgets to obtain the projection matrix directly from the experiment. It allows us to determine the Mueller matrix without precalibration of the setup, since the generated polarization states are fully determined by the azimuths of the wave plates. We calculate errors in determining the Mueller matrix and compare with other techniques. © 2014 Optical Society of America

OCIS codes: (120.2130) Ellipsometry and polarimetry; (260.5430) Polarization.
http://dx.doi.org/10.1364/JOSAA.31.000610

1. INTRODUCTION

The Mueller matrix of an optical element can provide us information about the retardation, the diattenuation, and the depolarization of light passing through that element [1,2]. Therefore, its determination has diverse applications ranging from tomography [3,4] to singular optics [5], liquid crystals [6], microelectronics [7], astronomy [8], and geoscience [9].

A three-component universal SU(2) polarization gadget developed by Simon and Mukunda can be used to generate any polarization state on the Poincaré sphere from a given input polarization state [10,11]. This gadget, called the Simon–Mukunda (SM) polarization gadget, consists of one half-wave plate (H) and two quarter-wave plates (Q); different polarization states can be obtained by changing the rotation of their fast axes appropriately [12]. The wave plates in the SM gadget can be placed in different configurations such as Q-H-Q, Q-Q-H, and H-Q-Q. However, we have used the Q-H-Q configuration only. In recent years, this universal SU(2) polarization gadget has been used for determining the polarization states of light in a variety of applications [13–16]. In lidar measurements of the depolarization of light due to polar mesospheric clouds, the instrument can introduce additional polarization changes. To compensate these changes, Hayman and Thayer have used the principle of the SM gadget [13,14]. Schilling *et al.* presented a theoretical scheme to determine the higher-order correlations of light using an SM gadget [15]. This gadget has also been used in measuring the Pancharatnam phase of a polarization state by Loredo *et al.* [16]. In the present study, we use it to find out the Mueller matrix of a given optical element. We have used two SM gadgets: one for the generation of input polarization states and another for obtaining the projection of each output state on a given set of four input states. To the best of our knowledge, this is the first experimental demonstration of determining the Mueller matrix with the SM gadget.

In general, the Mueller matrix is determined by measuring the output Stokes parameters of a given light beam, corresponding to four different input Stokes parameters. These parameters are obtained by measuring the intensities with different polarizations (horizontal, vertical, left circular, right circular, and both diagonals). This method is also known as the successive probing method [17] and needs 24 intensity measurements with known input Stokes parameters. In Mueller matrix imaging polarimetry, one can obtain the Mueller matrix by taking 16, 36, or 49 images [18], depending on error tolerances. In one of the earlier studies, to obtain the Mueller matrix, Azzam presented a technique called photopolarimetry that used two quarter-wave plates (one in polarizing optics and another in analyzing optics) rotating at speeds ω and 5ω [19].

Alternatively, the present study provides a novel and simple method for determining the Mueller matrix of an optical element using two SM gadgets. One of the main advantages of this method is that it does not require precalibration of the setup, since the generated polarization states are fully determined by the azimuths of the wave plates. In this paper, the theoretical background has been explained in Section 2, while the experimental demonstration is given in Section 3.

2. THEORETICAL ANALYSIS

The Stokes vector describes the complete polarization state of an electromagnetic wave. For an optical beam with a Stokes

vector (S) passing through an optical element, the output Stokes vector ($\tilde{S}$) can be written as

$$\tilde{S} = MS, \tag{1}$$

where S and $\tilde{S}$ are four element column vectors and M is a 4×4 matrix defined as a Mueller matrix. We form two matrices Ω and $\tilde{\Omega}$ by arranging four input and output Stokes vectors,

$$\Omega = [S_1 S_2 S_3 S_4], \qquad \tilde{\Omega} = [\tilde{S}_1 \tilde{S}_2 \tilde{S}_3 \tilde{S}_4]. \tag{2}$$

Using Eq. (1), the relationship between Ω and $\tilde{\Omega}$ can be written as

$$\tilde{\Omega} = M\Omega. \tag{3}$$

The four input states forming Ω must be on the surface of a Poincaré sphere. The projection of each output state $\tilde{S}_1$, $\tilde{S}_2$, $\tilde{S}_3$, $\tilde{S}_4$ on the corresponding input states S_1, S_2, S_3, S_4 gives 16 nonnegative real numbers that form the elements of projection matrix Λ. These elements are given by

$$\Lambda_{ij} = \frac{1}{2}(S_j)^T \tilde{S}_i = \frac{1}{2}\sum_{\alpha=1}^{4} S_j^\alpha \tilde{S}_i^\alpha, \tag{4}$$

where $i, j = 1$–4 and S_i^α denotes the αth element of the ith Stokes vector and Λ_{ij} is the projection of state $\tilde{S}_i$ on state S_j. Therefore, the projection matrix

$$\Lambda = \frac{1}{2}\Omega^T \tilde{\Omega} = \frac{1}{2}\Omega^T M \Omega, \tag{5}$$

and as a consequence, the Mueller matrix

$$M = 2(\Omega^T)^{-1}\Lambda\Omega^{-1}. \tag{6}$$

Thus, to obtain the Mueller matrix, one needs to choose four input states and determine the corresponding projection matrix. We have considered three regular tetrahedrons on the Poincaré sphere whose vertices form three sets of input states. The four vertices of these tetrahedrons uniformly cover the surface of a Poincaré sphere and give a maximum value to the determinant of Ω. We have selected these three tetrahedrons to optimize the errors in Mueller matrices [17]. The optimal input states $(1, q_i, u_i, v_i)^T$ for any polarimeter, which are the vertices of a regular tetrahedron on the Poincaré sphere, should obey the following conditions:

$$\sum_{i=1}^{4} q_i = \sum_{i=1}^{4} u_i = \sum_{i=1}^{4} v_i = 0; \tag{7}$$

$$\sum_{i=1}^{4} q_i u_i = \sum_{i=1}^{4} u_i v_i = \sum_{i=1}^{4} v_i q_i = 0; \tag{8}$$

and

$$\sum_{i=1}^{4} q_i^2 = \sum_{i=1}^{4} u_i^2 = \sum_{i=1}^{4} v_i^2 = \frac{4}{3}. \tag{9}$$

By solving these equations numerically, we have obtained a number of Ω [Eq. (2)] matrices or groups of optimal states for polarimetry.

The Stokes parameters (S_i^1, $i = 1$–4) representing the first tetrahedron are given by

$$\Omega^{(1)} = \begin{bmatrix} 1.000 & 1.000 & 1.000 & 1.000 \\ 1.000 & -0.333 & -0.333 & -0.334 \\ 0.000 & 0.943 & -0.472 & -0.471 \\ 0.000 & 0.000 & 0.816 & -0.816 \end{bmatrix}, \tag{10}$$

and the Euler angles corresponding to the four states are $(0,0,0)$, $(0,0,\kappa_1)$, $(0,-(2\pi/3),\kappa_1)$, and $(0,(2\pi/3),\kappa_1)$, where $\kappa_1 = \cos^{-1}(-0.333) = 109.47°$. The four vertices of the second tetrahedron are represented by the following Stokes parameters (S_i^2, $i = 1$–4):

$$\Omega^{(2)} = \begin{bmatrix} 1.000 & 1.000 & 1.000 & 1.000 \\ 0.680 & 0.430 & -0.730 & -0.390 \\ 0.701 & -0.752 & 0.392 & -0.350 \\ 0.214 & -0.500 & -0.560 & 0.852 \end{bmatrix}, \tag{11}$$

and the respective Euler angles are $(0,-(\pi/10.59),\kappa_2)$, $(0,-(\pi/5.35),-1.37\kappa_2)$, $(0,-(\pi/3.27),2.91\kappa_2)$, and $(0,-(\pi/1.61),2.40\kappa_2)$, where $\kappa_2 = \cos^{-1}(0.68) = 47.16°$. Similarly, the four vertices of the third tetrahedron are

$$\Omega^{(3)} = \begin{bmatrix} 1.000 & 1.000 & 1.000 & 1.000 \\ 0.580 & -0.580 & 0.580 & -0.580 \\ 0.576 & -0.580 & -0.576 & 0.580 \\ 0.580 & 0.572 & -0.572 & -0.580 \end{bmatrix}, \tag{12}$$

with corresponding Euler angles $(0,-(\pi/4),\kappa_3)$, $(0,-(\pi/1.30),2.30\kappa_3)$, $(0,(\pi/1.30),\kappa_3)$, and $(0,(\pi/4),2.30\kappa_3)$, where $\kappa_3 = \cos^{-1}(0.58) = 54.54°$.

The sum of four vertices forming these tetrahedrons is the origin of the Poincaré sphere and corresponds to the maximally mixed (completely unpolarized) state. In our study, we have considered Frobenius norms and condition numbers for these states, as the errors obtained in the Mueller matrices have a direct dependence on these numbers [17]. The optimal states should have a minimum norm and condition number along with the maximum determinant. For matrix Ω, norms and condition numbers are determined by

$$\|\Omega\|_F = \sqrt{\mathrm{trace}(\Omega^*\Omega)}, \tag{13}$$

$$c_F = \|\Omega\|_F * \|\Omega^{-1}\|_F. \tag{14}$$

Using Eqs. (13) and (14), we get the Frobenius norms as (2.8279, 2.8280, 2.8349), the corresponding condition numbers as (4.4729, 4.4727, 4.4640), and the absolute value of determinants as (3.0755, 3.1218, 3.0763), respectively, for the three

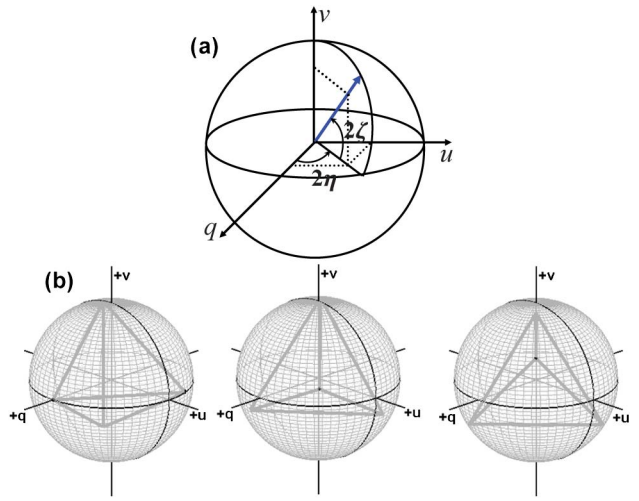

Fig. 1. Geometrical representation of (a) the Euler angles and (b) the three chosen tetrahedrons on the Poincaré sphere.

tetrahedrons. Although for all regular tetrahedrons, the norm, condition number, and determinant should be same, in this case they are slightly different. This is due to the rounding off in the Stokes parameters of the four vertices forming the tetrahedrons. We use the first SM gadget to generate four input polarization states $(S_1^i, S_2^i, S_3^i, S_4^i)$ corresponding to a particular tetrahedron. To generate a particular polarization state, the required orientations of the fast axes of the wave plates are given as the subscripts of Q, H, and Q [12]:

$$u(\xi,\eta,\zeta) = Q_{\frac{\pi}{4}+\frac{\xi}{2}} H_{\frac{-\pi}{4}+\frac{\xi+\eta-\zeta}{4}} Q_{\frac{\pi}{4}-\frac{\zeta}{2}}, \tag{15}$$

where ξ, η, ζ are the Euler angles corresponding to that polarization state. In Jones analysis, these angles represent the angle made by the frame of reference (ξ) from which observations are made (always zero when care is taken in aligning the setup), the phase lag between two orthogonal components of a field (η) in a given polarization state, and the rotation (ζ) of that polarization state from the horizontal or vertical direction, respectively. These angles can be shown on a Poincaré sphere as in Fig. 1(a). The angles of Q_1, H_1, $Q_{1'}$ in Table 1

Table 1. Angles of Rotation for Wave Plates in SM Gadget 1 to Generate the Four Vertices of Three Tetrahedrons

State S_i^k	θ_{iQ1}^k	θ_{iH1}^k	$\theta_{iQ1'}^k$
S_1^1	$\pi/4$	$-(\pi/4)$	$\pi/4$
S_2^1	$\pi/4$	$-(\pi/4) - (\kappa_1/4)$	$(\pi/4) - (\kappa_1/2)$
S_3^1	$\pi/4$	$-(\pi/4) - (\kappa_1/4) + (\pi/6)$	$(\pi/4) - (\kappa_1/2)$
S_4^1	$\pi/4$	$-(\pi/4) - (\kappa_1/4) - (\pi/6)$	$(\pi/4) - (\kappa_1/2)$
S_1^2	$\pi/4$	$-(\pi/4) - (\kappa_2/4) - (\pi/42.36)$	$(\pi/4) - (\kappa_2/2)$
S_2^2	$\pi/4$	$-(\pi/4) + (1.37\kappa_2/4) - (\pi/21.41)$	$(\pi/4) + (1.37\kappa_2/2)$
S_3^2	$\pi/4$	$-(\pi/4) - (2.90\kappa_2/4) + (\pi/13.08)$	$(\pi/4) - (2.90\kappa_2/2)$
S_4^2	$\pi/4$	$-(\pi/4) - (2.40\kappa_2/4) - (\pi/6.41)$	$(\pi/4) - (2.40\kappa_2/2)$
S_1^3	$\pi/4$	$-(\pi/4) - (\pi/16) - (\kappa_3/4)$	$(\pi/4) - (\kappa_3/2)$
S_2^3	$\pi/4$	$-(\pi/4) - (\pi/5.32) - (2.30\kappa_3/4)$	$(\pi/4) - (2.30\kappa_3/2)$
S_3^3	$\pi/4$	$-(\pi/4) + (\pi/5.32) - (\kappa_3/4)$	$(\pi/4) - (\kappa_3/2)$
S_4^3	$\pi/4$	$-(\pi/4) + (\pi/16) - (2.30\kappa_3/4)$	$(\pi/4) - (2.30\kappa_3/2)$

corresponding to S_i^k generate the ith state of the kth tetrahedron. Figure 1(b) shows the three chosen tetrahedrons on the Poincaré sphere.

To obtain the projection of an output state with an unknown optical element on a given set of input states, we have used another SM gadget. Let Λ_{ij}^k represent the projection of the output state $\tilde{S}_i^k$ on the input state S_j^k. To generate the required polarization state, we kept the angles in the first SM gadget as $\theta_{iQ_1}^k$, $\theta_{iH_1}^k$, and $\theta_{iQ_1'}^k$. To project the output state on the S_j^k state, we kept the angles in the second SM gadget as $\theta_{jQ_2}^k + (\pi/2)$, $\theta_{jH_2}^k + (\pi/2)$, and $\theta_{jQ_2'}^k + (\pi/2)$, which generates the inverse of S_j^k:

$$(Q_\theta)^{-1} = Q_{\frac{\pi}{2}+\theta}, (H_\theta)^{-1} = H_{\frac{\pi}{2}+\theta} \quad \text{and} \quad (Q'_\theta)^{-1} = Q'_{\frac{\pi}{2}+\theta}. \tag{16}$$

The 16 projection elements correspond to different orientations of wave plates form the projection matrix. We have made measurements with three sets of input states forming the vertices of a regular tetrahedron, and the corresponding projection matrices have been obtained. The reported Mueller matrix is the average of all three Mueller matrices corresponding to the three sets of input states. It should be pointed out that these projections can be taken on any four arbitrary polarization states corresponding to a regular tetrahedron.

3. EXPERIMENTAL DETAILS

The experimental setup for the generation of input polarization states and for obtaining the projection matrix for calculation of the Mueller matrix is shown in Fig. 2. A vertically polarized He–Ne laser with a wavelength of 632.8 nm and 35 mW of power is used for the experiment. The laser beam is allowed to pass through a polarizer P_1 to increase the ratio of vertical to horizontal polarization of the laser and to set the reference for a fast axis of all the polarizing elements. Vertically polarized light is then passed though the first SM gadget $(Q_1\ H_1\ Q_1')$ to generate four input states. These four generated states are further passed though a given sample whose Mueller matrix needs to be determined. The projections of the resulting output states on the four input states coming from the first SM gadget with respect to the initial polarization (set by P_1) are obtained by using a second SM gadget $(Q_2\ H_2\ Q_2')$ and an analyzer (P_2) whose transmission axis is kept parallel to P_1. This is accomplished by rotating the wave plates in the second SM gadget in a way that compensates the polarization changes occurring in the initial state. The angles are obtained simply by adding 90° to the angles used in the first SM gadget (Table 1). For example, to get the projections of the first output state, we fix the first set of angles $((\pi/4), -(\pi/4), (\pi/4))$, in the first SM gadget and take measurements

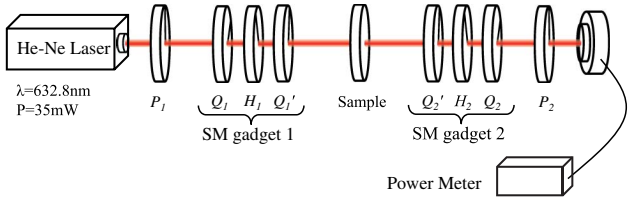

Fig. 2. Experimental setup for the determination of the Mueller matrix using two SM gadgets.

Table 2. Difference in the Frobenius Norms of Experimental and Theoretical Projection Matrices with Three Tetrahedrons[a]

Input	Free Space	HWP	QWP
Tetrahedron 1	0.019	0.017	0.019
Tetrahedron 2	0.012	0.176	0.011
Tetrahedron 3	0.011	0.087	0.036

[a]HWP, half-wave plate; QWP, quarter-wave plate.

of the four sets of angles with the second SM gadget obtained by adding 90° to the wave plate orientations. The observations are made with four sets of angles corresponding to four input states to obtain 16 nonnegative projection elements, as described in Eq. (4). The same procedure is repeated for other two tetrahedrons. These elements form a 4×4 projection matrix, which is required to determine the Mueller matrix by using Eq. (6). The resultant Mueller matrix is the average of three matrices corresponding to three sets of input states. An optical multimeter with an accuracy of 0.2% and resolution of 0.01 pW is used to measure the output power. We are using three known optical elements—free space, half-wave plate, and quarter-wave plate—as samples. We have used zero-order quartz wave plates from Melles Griot to make the SM gadgets and also as samples for measuring Mueller matrices to verify our method. These wave plates are mounted on computer-controlled motorized cylindrical rotation stages with a resolution of 0.04°. The quoted retardance tolerance of the wave plates is $\lambda/200$ to $\lambda/500$. To begin with, we have aligned the fast axes of all the wave plates as vertical. To ensure that the fast axes are perfectly vertical, we placed an analyzer with its fast axis perpendicular to the initial polarizer. Each optical element is separately aligned so that after the analyzer we have minimum power in the power meter.

4. RESULTS AND DISCUSSION

We have experimentally determined the projection matrices for free space, half-wave plates, and quarter-wave plates with their fast axes vertical. The projection matrices obtained, represented by the symbols $\Lambda_{\text{free}}^{(iE)}$, $\Lambda_H^{(iE)}$, $\Lambda_Q^{(iE)}$, where $i=1$–3, correspond to a particular tetrahedron. To obtain Mueller matrices for all the three optical elements, we have used Eq. (6). We have taken the average of three Mueller matrices corresponding to different tetrahedrons for a given sample. The average Mueller matrices from the experiment are denoted by $M_{\text{free}}^{(E)}, M_H^{(E)}, M_Q^{(E)}$ for free space (free), half-wave plate (H), and quarter-wave plate (Q), respectively. All of the projection and Mueller matrices are normalized with their first element.

To obtain the theoretical projection matrices, we have used Jones matrix analysis. The projection elements represent the fraction of the input intensity of a light beam after passing through all the optical elements. They have been obtained from the output Jones vectors of the beam. The Jones vector (J) of a light beam and the corresponding intensity (I) are given by

$$J=\begin{pmatrix}E_x\\E_y\end{pmatrix},\qquad I=|E_x|^2+|E_y|^2. \tag{17}$$

The output Jones vector has been determined from the product of the Jones matrices of all the optical components in the same order as shown in the experimental setup (Fig. 2):

$$J_{\text{output}}=J_{P_2}J_{Q_2}J_{H_2}J_{Q_2'}J_{\text{sample}}J_{Q_1'}J_{H_1}J_{Q_1}J_{P_1}J_{\text{input}}. \tag{18}$$

For a wave plate with retardation ϕ and fast axis orientation θ, the Jones matrix is given by [20]

$$J_R(\phi,\theta)=\begin{pmatrix}e^{\frac{i\phi}{2}}\cos^2(\theta)+e^{-\frac{i\phi}{2}}\sin^2(\theta) & (e^{\frac{i\phi}{2}}-e^{-\frac{i\phi}{2}})\cos(\theta)\sin(\theta)\\ (e^{\frac{i\phi}{2}}-e^{-\frac{i\phi}{2}})\cos(\theta)\sin(\theta) & e^{\frac{i\phi}{2}}\sin^2(\theta)+e^{-\frac{i\phi}{2}}\cos^2(\theta)\end{pmatrix}, \tag{19}$$

while for a polarizer with fast axis orientation θ, it is

$$J_p(\theta)=\begin{pmatrix}\cos^2(\theta) & \cos(\theta)\sin(\theta)\\ \cos(\theta)\sin(\theta) & \sin^2(\theta)\end{pmatrix}. \tag{20}$$

The 16 nonnegative and real projection elements are obtained with 16 sets of orientations of the wave plates in the SM gadgets. The theoretical projection matrices are denoted with the symbols $\Lambda_{\text{free}}^{(iT)}$, $\Lambda_H^{(iT)}$, $\Lambda_Q^{(iT)}$. The obtained theoretical projection matrices from the output Jones vectors are used in Eq. (6) to obtain the Mueller matrices $M_{\text{free}}^{(T)}$, $M_H^{(T)}$, $M_Q^{(T)}$. The experimentally obtained projection and Mueller matrices are in good agreement with the theoretical matrices. The differences in the Frobenius norms of the experimental and theoretical projection matrices have been given in Table 2 for free space, half-wave plate, and quarter-wave plate corresponding to all the three tetrahedrons. This shows the

Table 3. Experimental and Theoretical Mueller Matrices for Free Space, Half-Wave Plate (HWP), and Quarter-Wave Plate (QWP)

Mueller Matrix	Free Space	HWP	QWP
Experimental	$\begin{bmatrix}1.000 & -0.006 & 0.004 & 0.003\\ 0.000 & 0.994 & 0.012 & -0.006\\ 0.001 & -0.020 & 0.981 & 0.017\\ 0.000 & 0.001 & -0.008 & 1.006\end{bmatrix}$	$\begin{bmatrix}1.000 & -0.008 & -0.007 & -0.002\\ -0.004 & 1.010 & 0.008 & -0.008\\ -0.003 & -0.003 & -0.990 & -0.016\\ -0.002 & -0.002 & 0.001 & -1.008\end{bmatrix}$	$\begin{bmatrix}1.000 & -0.007 & -0.002 & 0.006\\ -0.008 & 1.006 & 0.012 & -0.013\\ -0.002 & 0.007 & -0.001 & 0.995\\ -0.006 & -0.002 & -0.994 & -0.001\end{bmatrix}$
Theoretical	$\begin{bmatrix}1 & 0 & 0 & 0\\ 0 & 1 & 0 & 0\\ 0 & 0 & 1 & 0\\ 0 & 0 & 0 & 1\end{bmatrix}$	$\begin{bmatrix}1 & 0 & 0 & 0\\ 0 & 1 & 0 & 0\\ 0 & 0 & -1 & 0\\ 0 & 0 & 0 & -1\end{bmatrix}$	$\begin{bmatrix}1 & 0 & 0 & 0\\ 0 & 1 & 0 & 0\\ 0 & 0 & 0 & 1\\ 0 & 0 & -1 & 0\end{bmatrix}$

deviation of the experimentally obtained projection matrices from the theoretical matrices. The experimental and the theoretical Mueller matrices are given in Table 3.

We have verified whether the experimental Mueller matrices are physically realizable or not with the calculations of the N-matrix discussed in [21]. The N-matrices for the three experimental Mueller matrices are given by

$$N_{\text{free}} = \begin{bmatrix} 1.000 & 0.008-0.002i & -0.010-0.000i & 0.999+0.013i \\ 0.008+0.002i & 0.006 & -0.013-0.004i & 0.011+0.001i \\ -0.010+0.000i & -0.013+0.004i & 0.000 & -0.004+0.005i \\ 0.999-0.013i & 0.011-0.001i & -0.004-0.005i & 1.006 \end{bmatrix},$$

$$N_H = \begin{bmatrix} 1.000 & 0.000-0.005i & -0.003+0.002i & -1.000-0.009i \\ 0.000+0.005i & -0.003 & 0.009+0.008i & -0.000+0.000i \\ -0.003-0.002i & 0.009-0.008i & -0.007 & -0.008+0.003i \\ -1.000+0.009i & -0.000-0.000i & -0.008-0.003i & 1.011 \end{bmatrix},$$

$$N_Q = \begin{bmatrix} 1.000 & 0.005-0.003i & 0.003+0.004i & -0.001+0.999i \\ 0.005+0.003i & -0.004 & 0.000-0.000i & -0.004+0.002i \\ 0.003-0.004i & 0.000+0.000i & -0.002 & -0.007+0.009i \\ -0.001-0.999i & -0.004-0.002i & -0.007-0.009i & 1.015 \end{bmatrix}.$$

The eigenvalues of the N-matrices are (−0.0117, 0.0036, 0.0176, **2.0024**), (−0.0189, 0.0039, 0.0111, **2.0055**), and (−0.0079, −0.0033, 0.0136, **2.0071**) for free space, half-wave plate, and quarter-wave plate, respectively. From these values, it is clear that all eigenvalues are real and only one eigenvalue is non-zero. This means that the N-matrices are projectors that are typical of nondepolarizing optical elements, as expected for the selected samples. Although some of the eigenvalues are negative, they are within the experimental errors. This shows that the obtained Mueller matrices represent real physical systems. Apart from this, we have also verified the following conditions:

$$N^2 = \text{tr}(N)\cdot N, \tag{21}$$

$$\text{tr}(MM^T) \le 4m_{00}^2. \tag{22}$$

Equation (21) also proves that the chosen optical elements are nondepolarizing elements. Equation (22) is a constraint on the degree of polarization for a physical system that is also satisfied in our case [22]. We have calculated the retardance for the half-wave plate and quarter-wave plate as 0.997π and 0.501π, respectively, by decomposing their Mueller matrices [1]. The deviations are within the tolerances given by the manufacturer.

5. ERROR ANALYSIS

The main sources of errors in this setup are the deviations in the fast axes of the wave plates from a vertical orientation and errors in their retardance. Along with these, fluctuations in the intensity of light and the measurements by the power meter also contribute to errors in the Mueller matrix of the optical element. We have neglected the error due to tilt of the wave plates, which has been taken care of in aligning the setup. The error analysis of the total system is done by the procedure followed in [23–25]. The whole experimental setup can be realized with the Jones matrices and written as [20]

$$\begin{aligned}\Lambda_{ij} = I[&J_P(\theta_{P2})\cdot J_R(\phi_{RQ'_2},\theta_{Q'_{2j}})\cdot J_R(\phi_{RH_2},\theta_{H_{2j}})\\ &\cdot J_R(\phi_{RQ_2},\theta_{Q_{2j}})\cdot O\cdot J_R(\phi_{RQ'_1},\theta_{Q'_{1i}})\cdot J_R(\phi_{RH_1},\theta_{H_{1i}})\\ &\cdot J_R(\phi_{RQ_1},\theta_{Q_{1i}})\cdot J_P(\theta_{P1})\cdot L],\end{aligned} \tag{23}$$

where I denotes the intensity recorded by the detector [Eq. (17)]. $J_P(\theta)$ and $J_R(\phi,\theta)$ denote Jones matrices for the polarizers rotated by an angle θ and the retarders with retardance ϕ and a fast axis orientation of θ, respectively. Subscripts RH and RQ denote the retardation by the half-wave plate and quarter-wave plate, respectively. $P1$ and $P2$ are the angles of rotation of the polarizers. O is the object for which the Mueller matrix is determined, and L denotes the laser. The laser L is represented by the Jones matrix for a vertically polarized light. The power meter values provide the elements of the projection matrix Λ_{ij}. Considering the errors introduced by the rotation stage mounts and optical components to be uncorrelated, we can write the variance σ introduced in Λ [24] as

$$\sigma_{\Lambda_{ij}} = \sqrt{\sum_{\text{all } x}\left(\frac{\partial\Lambda_{ij}}{\partial x}\right)^2\sigma_x^2}, \tag{24}$$

where x represents the variables from Eq. (23) with the tolerances

$$\begin{aligned}\Delta\theta_{P1} &= \Delta\theta_{P2} = \pm 0.03^\circ,\\ \Delta\phi_{RH} &= \Delta\phi_{RQ} = \pm 1.26^\circ,\\ \Delta\theta_{Ri} &= \Delta\theta_{Rj} = \pm 0.04^\circ, \quad \text{for } i,j = 1 \text{ to } 3.\end{aligned} \tag{25}$$

Using Eqs. (23)–(25), we can evaluate the errors corresponding to all the elements of the Λ matrix. After obtaining the error in the projection elements, we take into account the 1% intensity variation due to the laser and 0.2% due to the detector. We do the same error propagation analysis with the 16 variables present in projection matrix and obtain the error in Mueller matrix elements as

$$\sigma_M = \begin{bmatrix} 0.007 & 0.012 & 0.012 & 0.013 \\ 0.012 & 0.021 & 0.021 & 0.022 \\ 0.012 & 0.021 & 0.019 & 0.020 \\ 0.013 & 0.022 & 0.020 & 0.026 \end{bmatrix}. \quad (26)$$

In our experiment, the maximum errors obtained in the individual elements while calculating the Mueller matrices are ±0.020, ±0.016, and ±0.013 for free space, half-wave plate and quarter-wave plate, respectively. These errors are within the limits, as calculated in Eq. (26).

Now we compare our results with other methods based on polarimetry. Goldstein [26] determined a Mueller matrix with a maximum error of ±0.034 by using the dual-rotating retarder method. The maximum error in the Mueller matrix determined by Dev and Asundi [27] based on resultant Stokes vector measurements is ±0.0985. Bueno [28] obtained a Mueller matrix with a maximum error of ±0.014 by using liquid crystal variable retarders, whose retardance is varies by the applied voltage. Baba *et al.* determined a Mueller matrix with imaging polarimetry that uses variable rotators and retarders [29]. They have obtained a maximum error of ±0.0353 by taking 16 images and ±0.0138 while taking 36 images. Here, we have considered the Mueller matrix of *free space* for comparing the error with our method. The present method uses simple wave plates and requires just 16 measurements.

6. CONCLUSION

We have discussed a new and simple technique for determining the Mueller matrix of an optical element using two SM gadgets that does not require precalibration of the setup. The efficacy of the technique has been verified with three known optical elements, i.e., free space, half-wave plate, and quarter-wave plate. One may use this gadget in polarization state tomography [30] and quantum process tomography [31], which have diverse applications in quantum information and quantum computation.

REFERENCES

1. S. Y. Lu and R. A. Chipman, "Interpretation of Mueller matrices based on polar decomposition," J. Opt. Soc. Am. A **13**, 1106–1113 (1996).
2. S. Manhas, M. K. Swami, P. Buddhiwant, N. Ghosh, P. K. Gupta, and K. Singh, "Mueller matrix approach for determination of optical rotation in chiral turbid media in backscattering geometry," Opt. Express **14**, 190–202 (2006).
3. W. C. Kuo, N. K. Chou, C. Chou, C. M. Lai, H. J. Huang, S. S. Wang, and J. J. Shyu, "Polarization-sensitive optical coherence tomography for imaging human atherosclerosis," Appl. Opt. **46**, 2520–2527 (2007).
4. C. K. Hitzenberger, E. Götzinger, M. Sticker, M. Pircher, and A. F. Fercher, "Measurement and imaging of birefringence and optic axis orientation by phase resolved polarization sensitive optical coherence tomography," Opt. Express **9**, 780–790 (2001).
5. V. K. Jaiswal, R. P. Singh, and R. Simon, "Producing optical vortices through forked holographic grating: study of polarization," J. Mod. Opt. **57**, 2031–2038 (2010).
6. I. Moreno, A. Lizana, J. Campos, A. Márquez, C. Iemmi, and M. J. Yzuel, "Combined Mueller and Jones matrix method for the evaluation of the complex modulation in a liquid-crystal-on-silicon display," Opt. Lett. **33**, 627–629 (2008).
7. T. Novikova, A. De Martino, S. B. Hatit, and B. Drévillon, "Application of Mueller polarimetry in conical diffraction for critical dimension measurements in microelectronics," Appl. Opt. **45**, 3688–3697 (2006).
8. J. Tinbergen, *Astronomical Polarimetry* (Cambridge University, 1996).
9. K. J. Voss and E. S. Fry, "Measurement of the Mueller matrix for ocean water," Appl. Opt. **23**, 4427–4439 (1984).
10. R. Simon and N. Mukunda, "Minimal three-component SU(2) gadget for polarization optics," Phys. Lett. A **143**, 165–169 (1990).
11. V. Bagini, R. Borghi, F. Gori, M. Santarsiero, F. Frezza, G. Schettini, and G. Schirripa Spagnolo, "The Simon–Mukunda polarization gadget," Eur. J. Phys. **17**, 279–284 (1996).
12. B. Neethi Simon, C. M. Chandrashekar, and S. Simon, "Hamilton's turns as visual tool-kit for designing of single qubit unitary gates," Phys. Rev. A **85**, 022323 (2012).
13. M. Hayman and J. P. Thayer, "Lidar polarization measurements of PMCs," J. Atmos. Sol. Terr. Phys. **73**, 2110–2117 (2011).
14. M. Hayman and J. P. Thayer, "General description of polarization in lidar using Stokes vectors and polar decomposition of Mueller matrices," J. Opt. Soc. Am. A **29**, 400–409 (2012).
15. U. Schilling, J. V. Zanthier, and G. S. Agarwal, "Measuring arbitrary-order coherences: tomography of single-mode multiphoton polarization-entangled states," Phys. Rev. A **81**, 013826 (2010).
16. J. C. Loredo, O. Ortz, R. Weingärtner, and F. De Zela, "Measurement of Pancharatnam phase by robust interferometric and polarimetric methods," Phys. Rev. A **80**, 012113 (2009).
17. D. Layden, M. F. G. Wood, and I. A. Vitkin, "Optimum selection of input polarization states in determining the sample Mueller matrix: a dual photoelastic polarimeter approach," Opt. Express **20**, 20466–20481 (2012).
18. W. S. Bicke and W. M. Bailey, "Stokes vectors, Mueller matrices and polarized light scattering," Am. J. Phys. **53**, 468–478 (1985).
19. R. M. A. Azzam, "Photopolarimetric measurement of the Mueller matrix by Fourier analysis of a single detected signal," Opt. Lett. **2**, 148–150 (1978).
20. D. Goldstein, *Polarized Light* (Marcel Dekker, 2003).
21. R. Simon, "The connection between Mueller and Jones matrices of polarization optics," Opt. Commun. **42**, 293–297 (1982).
22. E. S. Fry and G. W. Kattawar, "Relationships between elements of the Stokes matrix," Appl. Opt. **20**, 2811–2814 (1981).
23. H. H. Ku, "Notes on the use of propagation of error formulas," J. Res. Natl. Bur. Standards C **70C**, 263–273 (1966).
24. A. C. Melissinos, *Experiments in Modern Physics* (Academic, 1966), Sec. 10.4, pp. 467–479.
25. D. F. V. James, P. G. Kwait, W. J. Munro, and A. G. White, "Measurement of qubits," Phys. Rev. A **64**, 052312 (2001).
26. D. H. Goldstein, "Mueller matrix dual-rotating retarder polarimeter," Appl. Opt. **31**, 6676–6683 (1992).
27. K. Dev and A. Asundi, "Mueller Stokes polarimetric characterization of transmissive liquid crystal spatial light modulator," Opt. Lasers Eng. **50**, 599–607 (2012).
28. J. M. Bueno, "Polarimetry using liquid-crystal variable retarders: theory and calibration," J. Opt. A **2**, 216–222 (2000).
29. J. S. Baba, J. R. Chung, A. H. DeLaughter, B. D. Cameron, and G. L. Cote, "Development and calibration of an automated Mueller matrix polarization imaging system," J. Biomed. Opt. **7**, 341–349 (2002).
30. A. Ling, K. P. Soh, A. L. Linares, and C. Kurtsiefer, "Experimental polarization state tomography using optimal polarimeters," Phys. Rev. A **74**, 022309 (2006).
31. M. W. Mitchell, C. W. Ellenor, S. Schneider, and A. M. Steinberg, "Diagnosis, prescription, and prognosis of a Bell-state filter by quantum process tomography," Phys. Rev. Lett. **91**, 120402 (2003).